Supplementary Information for

Simultaneous Prediction of Three Key Li-Ion Battery Indicators through Multi-Task Learning

Minjeong Gong[a], Yoonjung Choi[a], Han Mo Yang[b], Sang Bok Ma[b], Dong-Hwa Seo[a]*

Affiliation

[a] *Department of Materials Science and Engineering, Korea Advanced Institute of Science and Technology (KAIST), 291 Daehak-ro, Yuseong-gu, Daejeon 34141, Republic of Korea*

[b] *Battery Tech Department, SK ecoplant, 19 Yulgok-ro 2-gil, Jongno-gu, Seoul 03143, Republic of Korea*

* Corresponding author: dseo@kaist.ac.kr (Prof. D.-H. Seo)

Supplementary Note S1. Input feature generation from diagnostic protocol data

Features were systematically extracted from the voltage response recorded during the diagnostic protocol test, categorized into three primary types: instantaneous voltages, resistances, and voltage distribution characteristics. The instantaneous voltages included $V_{0.1s}$ and V_{5s}, where $V_{x\,s}$ denotes the voltage measured x seconds after the onset of a current pulse or rest time. Alongside these values, resistances were derived, namely $R_{0\text{-}0.1s}$ and $R_{0.1\text{-}5s}$, to capture both ohmic and polarization behaviors during each step. Resistances were calculated as follows:

$$R_{x-y\,s} = \frac{|V_{x\,s} - V_{y\,s}|}{current}$$

To further characterize the electrochemical dynamics, the distribution of voltage during each step was quantified using the skewness and kurtosis of the voltage response for every current pulse and rest time. Specifically, skewness measures the asymmetry of the recorded voltages, reflecting the direction and degree of bias in the voltage response, while kurtosis indicates the tailedness or peakedness of the distribution, capturing the sharpness and intensity of the voltage transitions.

Beyond these step-specific metrics, additional relational features were generated to express dependencies across varying C-rate and current directions. These included the end voltage difference of each pulse to account for the hysteresis effect (hyst), as well as the resistance ratio between charging and discharging (R_ratio) at identical C-rates. The sensitivity of the resistance to current magnitude was also incorporated by calculating the resistance ratio between the 1.65 and 2.0 C-rate. Given the high dimensionality of the resulting feature set, a systematic labeling convention—(C-rate)_(current direction)_(pulse or rest)_(value)—was adopted to ensure consistent identification and management of each feature associated with the diverse diagnostic protocols. Specifically, the C-rate component is comprised of two distinct values: 1.65 and 2.0 C, while the current direction is designated as ‘ch’ for charging or ‘dch’ for discharging. To distinguish between operational states, the abbreviations ‘P’ and ‘R’ are used to indicate pulse and rest time, respectively. Finally, the value component specified the type of metric extracted, such as V for instantaneous voltage, R for resistance, hyst for hysteresis effect, or R_ratio, allowing for a precise mapping of each feature to its corresponding condition.

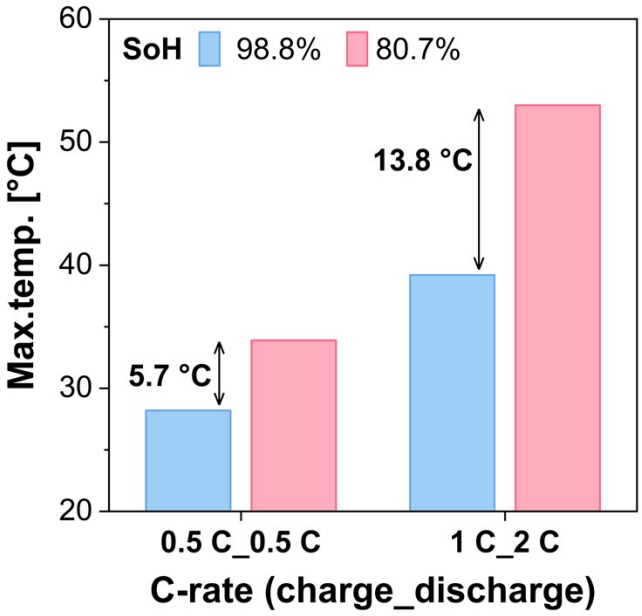

Fig. S1 The Max. temp. comparison as cell degradation depending on the current density (a) 0.5 C-rate charge and 0.5 C-rate discharge (b) 1 C-rate charge and 2 C-rate discharge

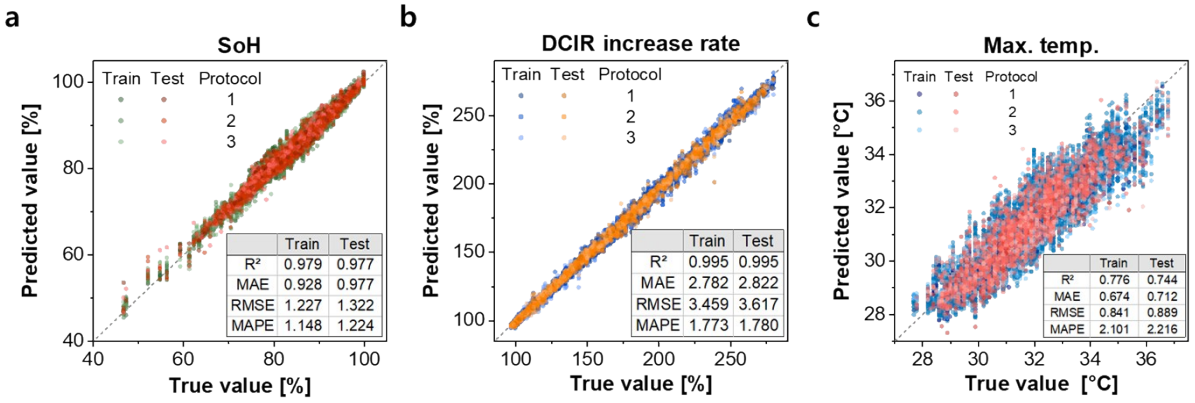

Fig. S2 The prediction performance of a single-target neural network model consisting of 5 hidden layers with 256 nodes each **(a)** SoH, **(b)** DCIR increase rate, and **(c)** Max. temp.

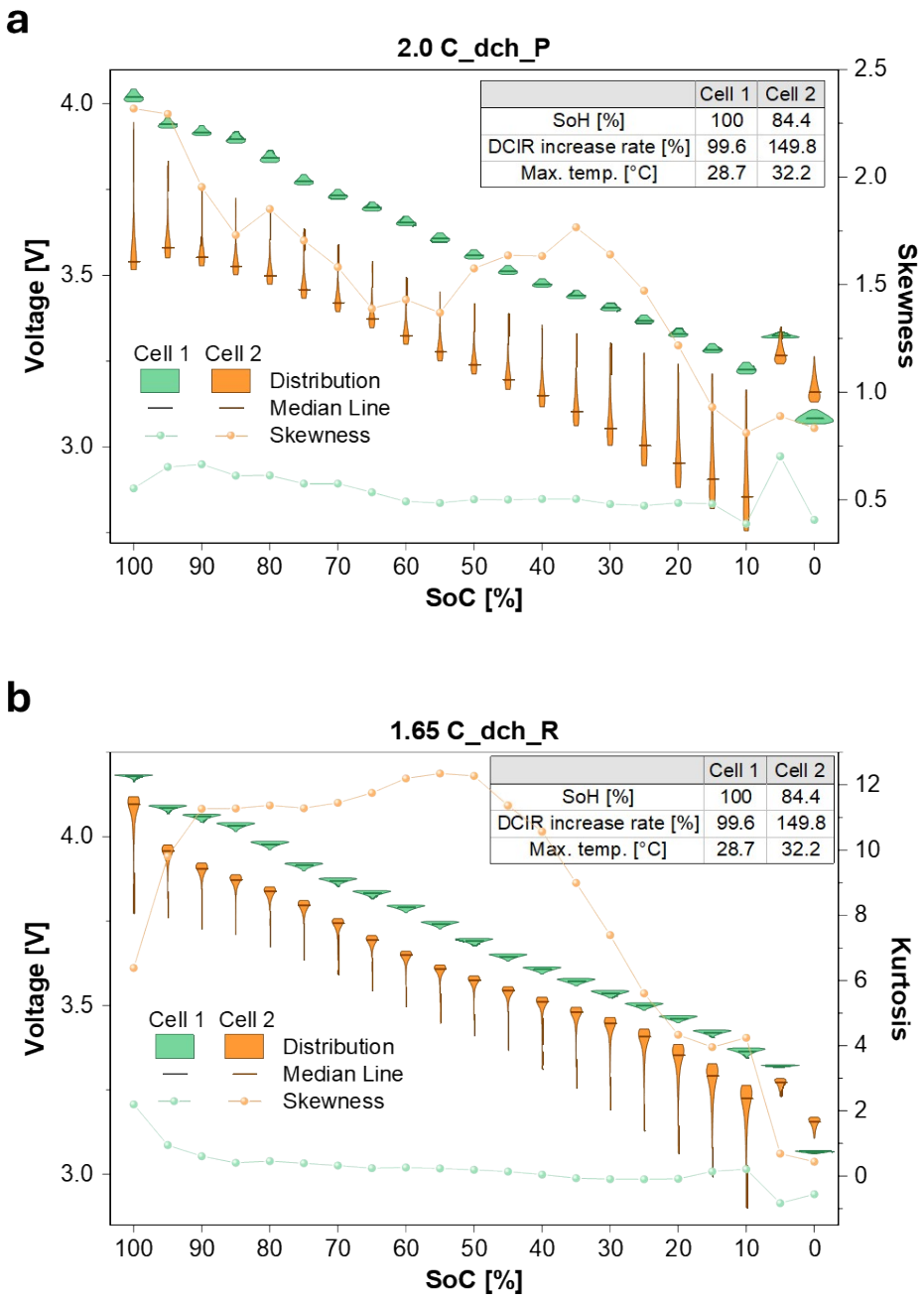

Fig. S3 Comparison of high-impact features from IG analysis across the SoC **(a)** 2.0C_dch_P_skew **(b)** 1.65C_dch_R_kurt

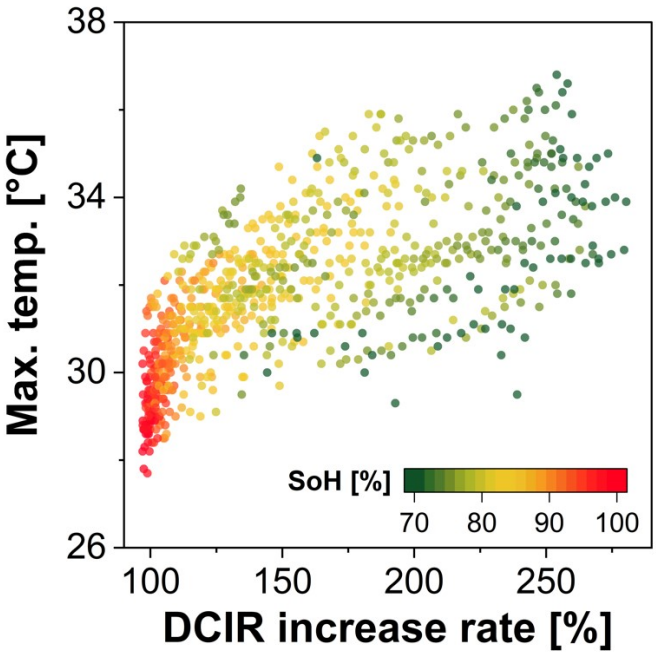

Fig. S4 The relationship between Max. temp. and DCIR increases the rate with SoH-based color mapping.

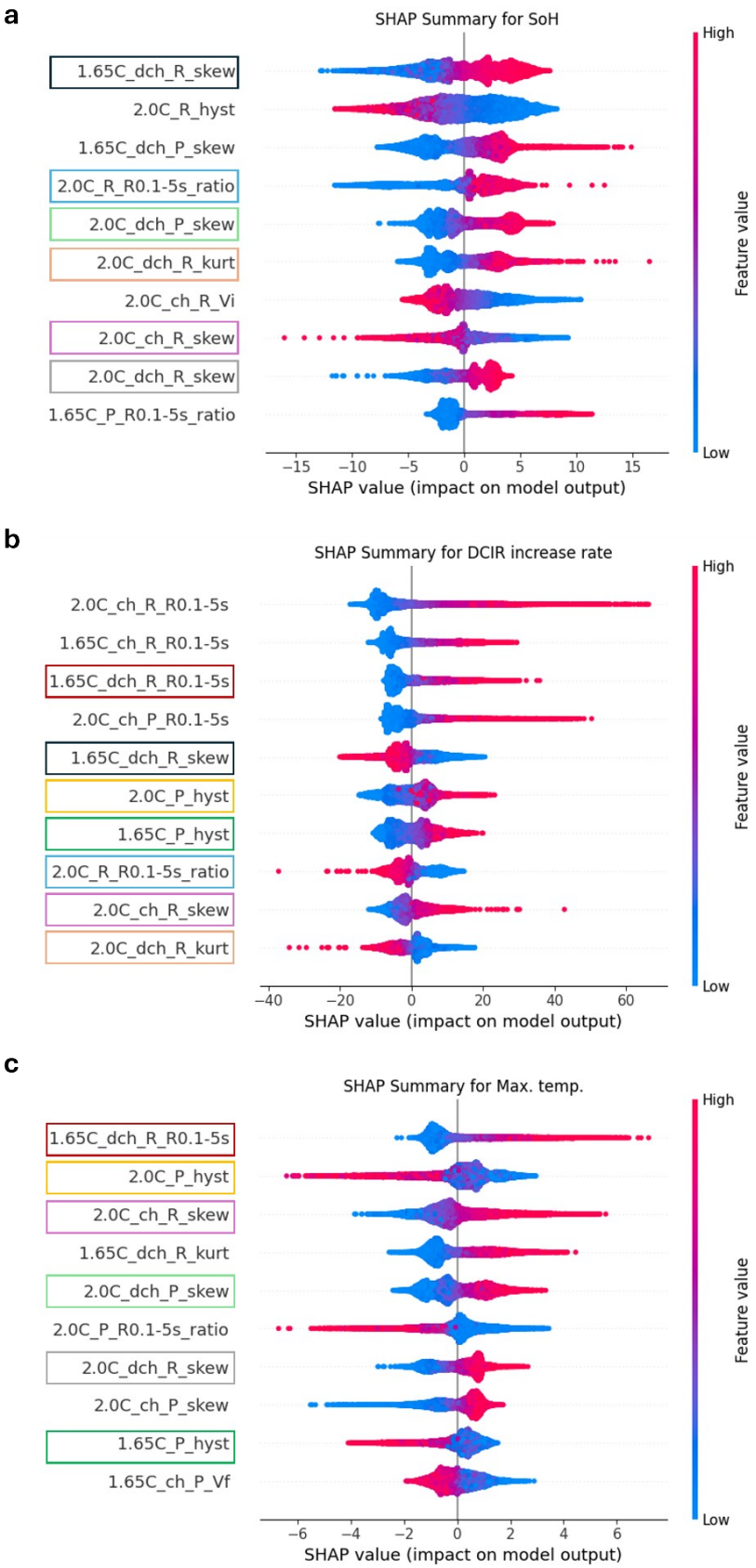

Fig. S5 Top 10 features with the highest SHAP values for MTL model (a) SoH, (b) DCIR increase rate, and (c) Max. temp. To approximate the conditional expectation of the SHAP values, 1,000 randomly selected samples as the background distribution were utilized.

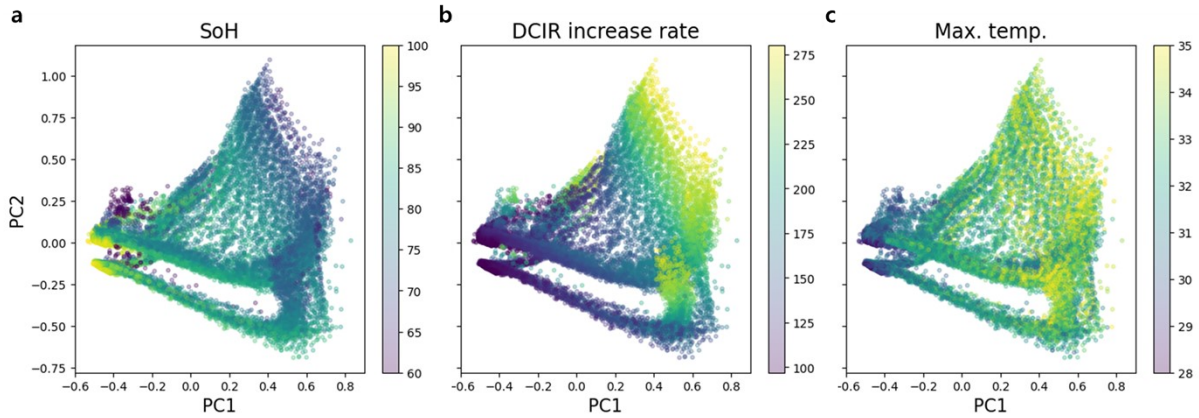

Fig. S6 PCA results obtained from 7 selected features derived from the top 4 IG values per battery indicator prediction. Color mappings were represented (a) SoH, (b) DCIR increase rate, and (c) Max. temp.

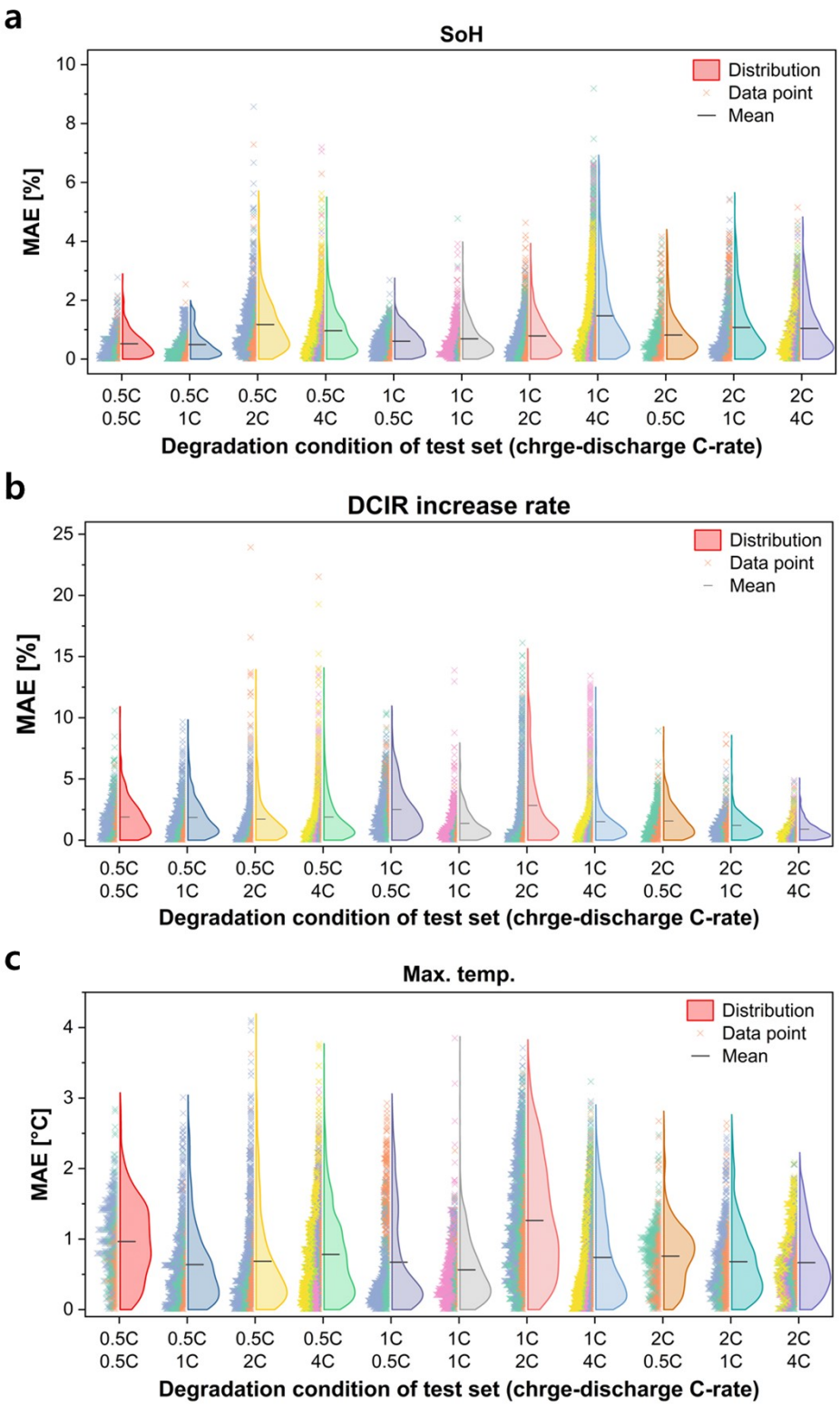

Fig. S7 The Mean Absolute Error (MAE) of the cell-wise split evaluation. For each test, all degradation-cycle data from one physical cell were excluded from the training set and used exclusively as the test set, while the model was trained using data from the remaining cells. The color of each data point indicates the held-out physical cell. (a) SoH, (b) DCIR increase rate, (c) Max. temp.

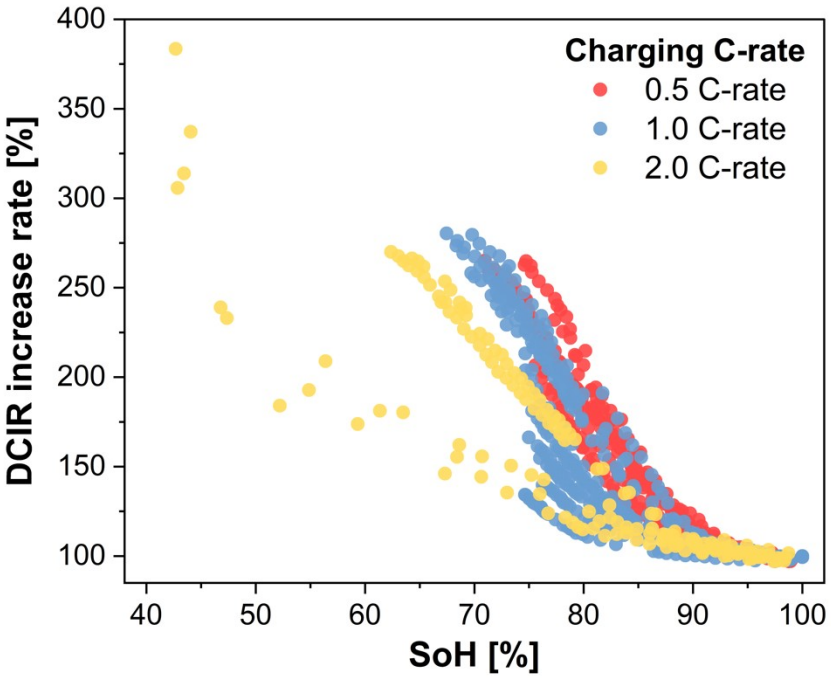

Fig. S8 The relationship between SoH and DCIR increase rate depending on the charging C-rate during the degradation cycle.

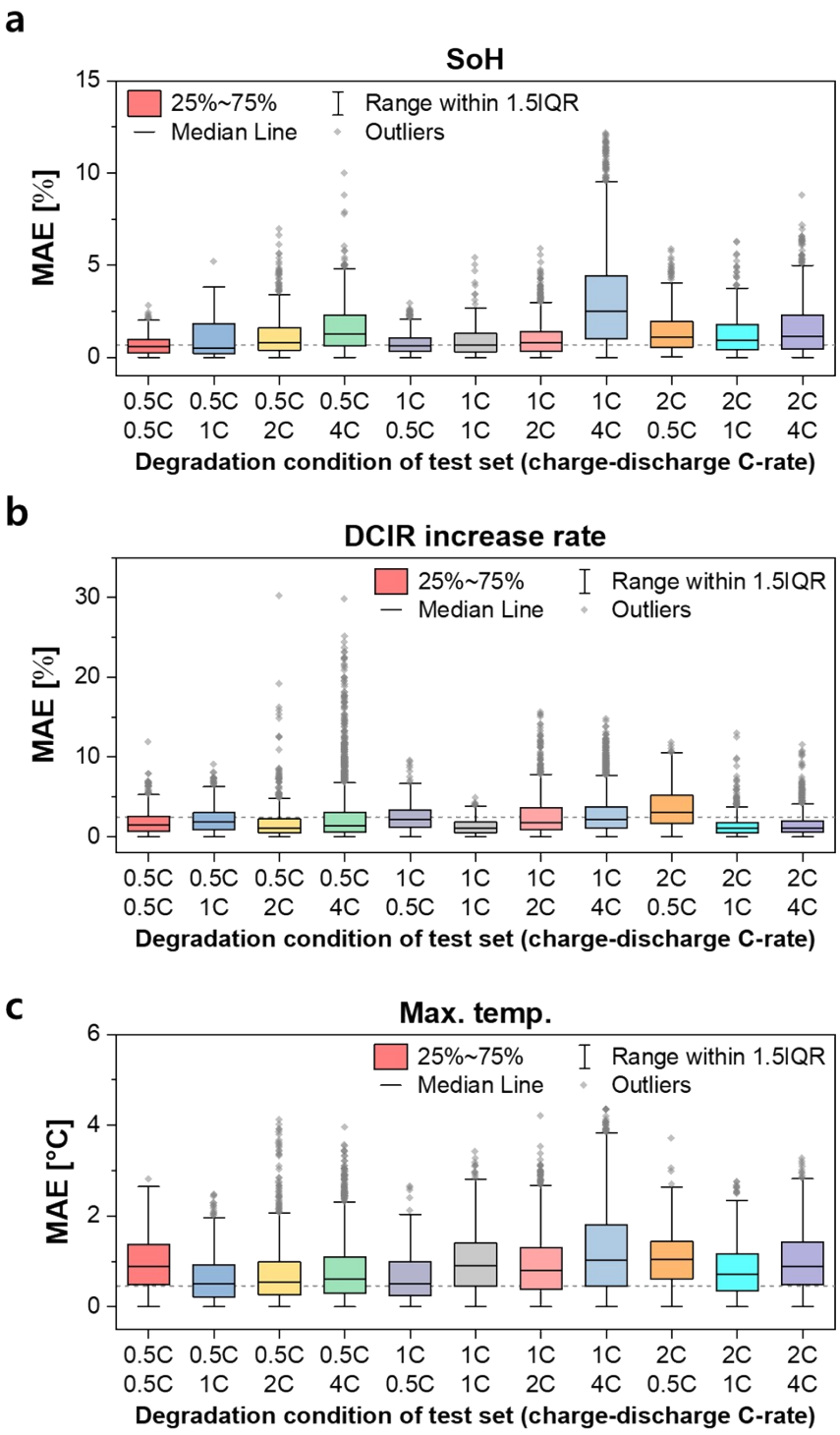

Fig. S9 The Mean Absolute Error (MAE) of the test dataset on degradation cycles excluded from the training set, which utilized all conditions except those on the x-axis. (a) SoH, (b) DCIR increase rate, (c) Max. temp.

Table S1. Selected features of STL model for each target prediction

SoH	DCIR increase rate	Max. temp.
2.0C_ch_R_$R_{0\text{-}0.1s}$	2.0C_ch_R_$R_{0\text{-}0.1s}$	2.0C_dch_P_skew
2.0C_P_hyst	1.65C_dch_P_$R_{0.1\text{-}5s}$	2.0C_ch_R_$R_{0\text{-}0.1s}$
1.65C_dch_R_$R_{0\text{-}0.1s}$	2.0C_R_hyst	2.0C_P_hyst
2.0C_ch_P_$R_{0.1\text{-}5s}$	1.65C_dch_P_$R_{0\text{-}0.1s}$	1.65C_dch_P_$R_{0\text{-}0.1s}$
2.0C_dch_P_$R_{0\text{-}0.1s}$	2.0C_ch_P_$R_{0.1\text{-}5s}$	2.0C_R/1.65C_R_dch_R
1.65C_dch_P_$R_{0.1\text{-}5s}$	2.0C_P_hyst	2.0C_ch_P_$R_{0.1\text{-}5s}$
1.65C_dch_P_skew	2.0C_ch_R_skew	2.0C_ch_R_skew
2.0C_ch_P_V_{5s}	2.0C_ch_P_V_{5s}	1.65C_R_R_ratio
2.0C_ch_R_skew	2.0C_dch_P_V_{5s}	2.0C_ch_P_skew
2.0C_dch_R_$R_{0\text{-}0.1s}$	1.65C_dch_R_skew	2.0C_dch_P_V_{5s}
1.65C_dch_R_skew	1.65C_R_hyst	2.0C_ch_P_V_{5s}
2.0C_ch_P_skew	2.0C_R/1.65C_R_ch_R	1.65C_dch_P_$R_{0.1\text{-}5s}$
2.0C_dch_P_V_{5s}	2.0C_ch_P_skew	1.65C_R_hyst
1.65C_P_R_ratio	1.65C_R_R_ratio	1.65C_P_R_ratio
1.65C_R_R_ratio	1.65C_dch_P_skew	1.65C_dch_P_skew
		2.0C_R_hyst

Table S2. Model and hyperparameters for SoH prediction model

Model	RandomForestRegressor
Max_depth	18
min_samples_leaf	2
min_samples_split	2
n_estimators	261
bootstrap	False
max_features	0.5

Table S3. Model and hyperparameters for DCIR increase rate prediction model

Model	RandomForestRegressor
Max_depth	18
min_samples_leaf	10
min_samples_split	20
n_estimators	761
bootstrap	True
max_features	0.7957098983397253

Table S4. Model and hyperparameters for Max. temp. prediction model

Model	ExtraTreesRegressor
Max_depth	28
Max_features	0.8844947491244998
n_estimators	240
bootstrap	True
min_samples_leaf	4
min_samples_split	12

Table S5. MAE of 10-fold cross validation results for MTL framework

	SoH	DCIR increase rate	Max. temp.
Fold 1	0.7115	1.4300	0.4623
Fold 2	0.6708	1.3484	0.4270
Fold 3	0.6892	1.4087	0.4471
Fold 4	0.9571	1.4607	0.5289
Fold 5	0.7204	1.6065	0.4975
Fold 6	0.7417	1.3824	0.4459
Fold 7	0.7222	1.4546	0.4288
Fold 8	0.7025	1.7466	0.5066
Fold 9	0.6767	1.6032	0.5344
Fold 10	0.7096	1.4044	0.4516
Mean	0.7302	1.4845	0.4730

Table S6. 10-fold cross validation results of MTL framework

	SoH	DCIR increase rate	Max. temp.
R^2 score	0.9870	0.9983	0.8744
MAE	0.7302	1.4845	0.4730
RMSE	0.9755	2.1050	0.6262
MAPE	0.9000	0.9529	1.4832

Table S7. 10-fold cross validation results of STL models

	SoH	DCIR increase rate	Max. temp.
R^2 score	0.9758	0.9930	0.7860
MAE	0.9024	2.5498	0.6438
RMSE	1.3343	4.2614	0.8194
MAPE	1.1219	1.4976	2.0068